STRUCTURAL BIOLOGY COMMUNICATIONS

ISSN 2053-230X

Received 5 October 2017
Accepted 28 March 2018

Edited by S. Sheriff, Bristol-Myers Squibb, USA

Keywords: structural genomics; Seattle Structural Genomics Center for Infectious Disease; *Burkholderia thailandensis*; chorismate mutase; isomerases.

PDB reference: chorismate mutase from *Burkholderia thailandensis*, 6cnz

Supporting information: this article has supporting information at journals.iucr.org/f

Crystal structure of chorismate mutase from *Burkholderia thailandensis*

Oluwatoyin A. Asojo,[a]* David M. Dranow,[b,c] Dmitry Serbzhinskiy,[c] Sandhya Subramanian,[c,d] Bart Staker,[c,d] Thomas E. Edwards[b,c] and Peter J. Myler[c,d]

[a]National School of Tropical Medicine, Baylor College of Medicine, 1102 Bates Avenue Suite 550, Mail Stop BCM320, Houston, TX 77030-3411, USA, [b]Beryllium Discovery Corporation, Bainbridge Island, WA 98110, USA, [c]Seattle Structural Genomics Center for Infectious Disease (SSGCID), Seattle, Washington, USA, and [d]Center for Infectious Disease Research, 307 Westlake Avenue North Suite 500, Seattle, WA 98109, USA. *Correspondence e-mail: asojo@bcm.edu

Burkholderia thailandensis is often used as a model for more virulent members of this genus of proteobacteria that are highly antibiotic-resistant and are potential agents of biological warfare that are infective by inhalation. As part of ongoing efforts to identify potential targets for the development of rational therapeutics, the structures of enzymes that are absent in humans, including that of chorismate mutase from *B. thailandensis*, have been determined by the Seattle Structural Genomics Center for Infectious Disease. The high-resolution structure of chorismate mutase from *B. thailandensis* was determined in the monoclinic space group $P2_1$ with three homodimers per asymmetric unit. The overall structure of each protomer has the prototypical AroQγ topology and shares conserved binding-cavity residues with other chorismate mutases, including those with which it has no appreciable sequence identity.

1. Introduction

Burkholderia thailandensis is a less infective member of the *Burkholderia* genus of proteobacteria that is often used as a model for more virulent members of this genus (Haraga *et al.*, 2008). *Burkholderia* are nonfermenting motile Gram-negative bacteria, and infectious members such as *B. mallei*, *B. pseudomallei* and *B. cepacia* are highly antibiotic-resistant and as such could be used as biological agents targeting humans and animals (Yabuuchi *et al.*, 1992; Sawana *et al.*, 2014). *B. cepacia* and 16 other closely related species known as the *B. cepacia* complex (BCC) cause severe and often fatal pulmonary infections in cystic fibrosis patients and other immunocompromised individuals (Mahenthiralingam *et al.*, 2002; Agodi *et al.*, 2002; Speert *et al.*, 2002). Another species, *B. pseudomallei*, causes up to 20% of all community-acquired septicemias, notably a lethal form of melioidosis (Limmathurotsakul & Peacock, 2011). Other *Burkholderia* species cause infections in animals (*B. mallei*) and plants (*B. glumae* and *B. gladioli*), and the BCC species are infectious by inhalation (Whitlock *et al.*, 2007; Cui *et al.*, 2016). New antibacterials against *Burkholderia* need to be developed owing to the importance of these species. One promising approach is to target enzymes that have shown promise in other bacteria and are absent in mammals, for example the enzymes of the shikimate pathway, which is important for the biochemical synthesis of aromatic amino acids, folic acid, ubiquinone and other aromatic compounds (Mousdale & Coggins, 1991; Abell, 1999; Haslam, 1993; Coggins *et al.*, 2003). The first committed step in the shikimate pathway is the Claisen rearrangement of chorismate to prephenate, which is catalysed by chorismate

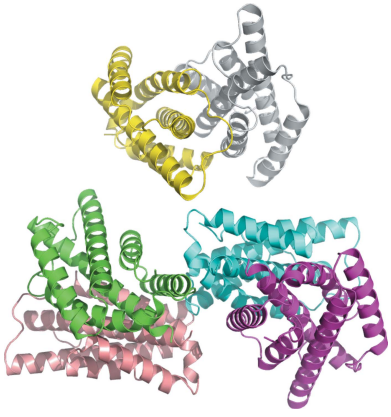

Table 1
Macromolecule-production information.

Source organism	*B. thailandensis* E264 (strain E264/ATCC 700388/DSM 13276/CIP 106301)
DNA source	Genomic DNA provided by Dr Joseph Mougous, University of Washington
Forward primer	CTCACCACCACCACCACCATATGGCCGACG GCGACGATACC
Reverse primer	ATCCTATCTTACTCACTTAGCCGACGGCGC TGGCGCC
Cloning vector	pBG1861
Expression vector	pBG1861
Expression host	*E. coli* BL21(DE3)R3 Rosetta
Complete amino-acid sequence of the construct produced†	MAHHHHHHMADGDDTALTNLVALASQRLAL AEPVAHWKWINRKPISDPPREAALLTDV EKRATANGVDPAYARTFFDDQIAASKQL QNALFATWRATHGPEGPAPDLATSTRPQ LDRLTQSLIAALARVAPLRDAPDCPSRL ARSIANWKTLTRYDSAQKDALGTALSHV CAAGGASAVG

† The noncleavable 6×His fusion tag is underlined.

mutase, which is also known as hydroxyphenylpyruvate synthase. Chorismate mutases occur in two classes: the monofunctional AroH class and the more common, sometimes bifunctional AroQ class. Members of the AroH class have a trimeric α/β-barrel topology, while the AroQ class form dimeric helical bundles. Subclasses of the AroQ class include AroQγ and AroQα, with roles in virulence (Haslam, 1993; Roberts *et al.*, 1998). Here, we present the recombinant production and structural analysis of an AroQγ chorismate mutase from *B. thailandensis*.

2. Materials and methods

2.1. Macromolecule production

Chorismate mutase from *B. thailandensis* was cloned, expressed and purified by the Seattle Structural Genomics Center for Infectious Disease (SSGCID; Myler *et al.*, 2009; Stacy *et al.*, 2011) following standard protocols described previously (Bryan *et al.*, 2011; Choi *et al.*, 2011; Serbzhinskiy *et al.*, 2015). Briefly, genomic DNA from *B. thailandensis* E264 (Kim *et al.*, 2005) was kindly provided by Dr Joseph Mougous, University of Washington. The signal-peptide-cleaved mature protein (UniProt Q2SY64) encoding amino acids 32–202 was PCR-amplified from genomic DNA using the primers shown in Table 1. The resultant amplicon was cloned into the ligation-independent cloning (LIC; Aslanidis & de Jong, 1990) pET-14b-based expression vector pBG1861, which was kindly provided by Wesley Van Voorhis, University of Washington, encoding a noncleavable 6×His fusion tag (MAHHHHHHM-ORF). Plasmid DNA was transformed into chemically competent *Escherichia coli* BL21(DE3)R3 Rosetta cells. The cells were tested for expression and a 2 l culture was grown using auto-induction medium (Studier, 2005) in a LEX Bioreactor (Epiphyte Three Inc.). The expression clone was assigned the SSGCID target identifier ButhA.00160.a.B2, and the clone and purified protein are available at https://apps.sbri.org/SSGCIDTargetStatus/Target/ButhA.00160.a.

Table 2
Crystallization.

Method	Sitting-drop vapor diffusion
Plate type	96-well Compact 300, Rigaku
Temperature (K)	290
Protein concentration (mg ml^{-1})	20 (diluted from 58.13)
Buffer composition of protein solution	20 m*M* HEPES pH 7.0, 300 m*M* NaCl, 5% glycerol, 1 m*M* TCEP
Composition of reservoir solution	JCSG-*plus* condition C3: 20%(*w*/*v*) PEG 3350, 200 m*M* ammonium nitrate
Volume and ratio of drop	0.4 µl:0.4 µl
Volume of reservoir (µl)	80

Table 3
Data collection and processing.

Values in parentheses are for the outer shell.

Diffraction source	Beamline 21-ID-G, APS
Wavelength (Å)	0.97857
Temperature (K)	100
Detector	MAR Mosaic 300 mm CCD
Crystal-to-detector distance (mm)	275
Rotation range per image (°)	1.0
Total rotation range (°)	180
Exposure time per image (s)	1.5
Space group	$P2_1$
a, *b*, *c* (Å)	51.71, 121.38, 88.67
α, β, γ (°)	90, 99.99, 90
Mosaicity (°)	0.2
Resolution range (Å)	50.00–2.15 (2.21–2.15)
Total No. of reflections	221537 (16462)
No. of unique reflections	57764 (4233)
Completeness (%)	98.7 (98.6)
Multiplicity	3.80 (3.89)
$\langle I/\sigma(I)\rangle$	18.47 (2.78)
$R_{\rm r.i.m.}$	0.061 (0.54)
Overall *B* factor from Wilson plot (Å^2)	25.7
PDB code	6cnz

The protein was purified by a two-step protocol consisting of immobilized metal (Ni^{2+})-affinity chromatography (IMAC) followed by size-exclusion chromatography (SEC). All chromatography runs were performed on an ÄKTApurifier 10 (GE) using automated IMAC and SEC programs according to previously described procedures (Bryan *et al.*, 2011). The final SEC was performed on a HiLoad 26/600 Superdex 75 column (GE Healthcare) using a mobile phase consisting of 300 m*M* NaCl, 20 m*M* HEPES pH 7.0, 5% glycerol, 1 m*M* TCEP. Peak fractions eluted as a single peak consistent with a monomeric enzyme. The peak fractions were pooled and analysed for the presence of the protein of interest using SDS–PAGE. The peak fractions were concentrated to 58.13 mg ml^{-1} using an Amicon purification system (Millipore). Aliquots of 200 µl were flash-frozen in liquid nitrogen and stored at −80°C until use for crystallization.

2.2. Crystallization

The protein was crystallized using established crystallization approaches at the SSGCID. Briefly, the protein was diluted to 20 mg ml^{-1} and single crystals were obtained by vapor diffusion in sitting drops directly from JCSG-*plus* condition C3 (Table 2).

Table 4
Structure solution and refinement.

Values in parentheses are for the outer shell.

Resolution range (Å)	50.0–2.15 (2.204–2.150)
Completeness (%)	98.7 (98.6)
No. of reflections, working set	57741 (3941)
No. of reflections, test set	1968 (139)
Final R_{cryst}	0.164 (0.218)
Final R_{free}	0.216 (0.276)
Cruickshank DPI	0.2392
No. of non-H atoms	
Protein	7226
Nitrate	76
Cryoprotectant (EDO)	28
Water	470
Total	7800
R.m.s. deviations	
Bonds (Å)	0.007
Angles (°)	0.865
Average *B* factors (Å^2)	
Protein	43.0
Nitrate	61.6
Cryoprotectant (EDO)	56.1
Water	42.4
Ramachandran plot	
Most favored (%)	98.21
Allowed (%)	1.16

2.3. Data collection and processing

Data-collection and processing information is reported in Table 3. Data were integrated and scaled with *XDS* and *XSCALE* (Kabsch, 2010). X-ray diffraction images are available for this entry, which was previously refined as PDB entry 4oj7 and is now updated as PDB entry 6cnz, at https://proteindiffraction.org/project/4oj7/.

2.4. Structure solution and refinement

The structure was solved by molecular replacement with *MOLREP* (Vagin & Teplyakov, 2010; Lebedev *et al.*, 2008). The search model was chorismate mutase from *Mycobacterium tuberculosis* (PDB entry 2f6l; 31% sequence identity; Kim *et al.*, 2006). Initial refinement was carried out with *REFMAC* 5.8.0049 (Murshudov *et al.*, 2011) with TLS and manual refinement in *Coot* (Emsley & Cowtan, 2004; Emsley *et al.*, 2010). The quality of the structure was checked by *MolProbity* (Chen *et al.*, 2010). The coordinates were initially deposited as PDB entry 4oj7; after initial review of the manuscript, further model building and structure refinement were performed using the *PHENIX* package (Terwilliger *et al.*, 2008) and the coordinates were updated as PDB entry 6cnz. The resulting structure-refinement data are provided in Table 4. All structural figures were generated using *PyMOL* (http://www.pymol.org).

3. Results and discussion

The crystal structure of chorismate mutase from *B. thailandensis* was solved in the monoclinic space group $P2_1$ with three homodimers per asymmetric unit (Fig. 1). The homodimer buries 2340 Å^2 of surface. The dimer offers opportunities for the future study of allostery and chorismate biosynthesis in *Burkholderia* as previously investigated for *Geobacillus* sp. (Nazmi *et al.*, 2016) and *Mycobacterium tuberculosis* (Munack *et al.*, 2016). The structures most similar to chorismate mutase from *B. thailandensis* were identified by

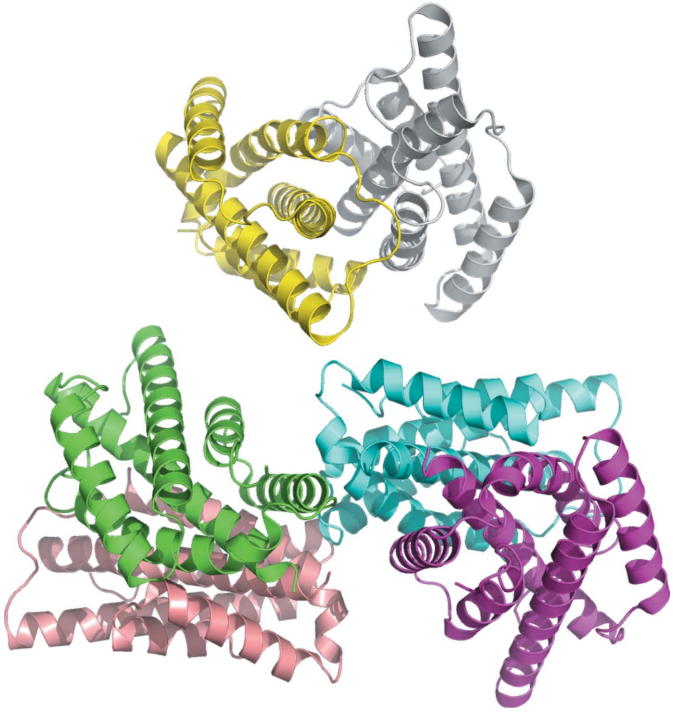

Figure 1
The asymmetric unit of the 2.15 Å resolution crystal structure of chorismate mutase from *B. thailandensis* contains three homodimers.

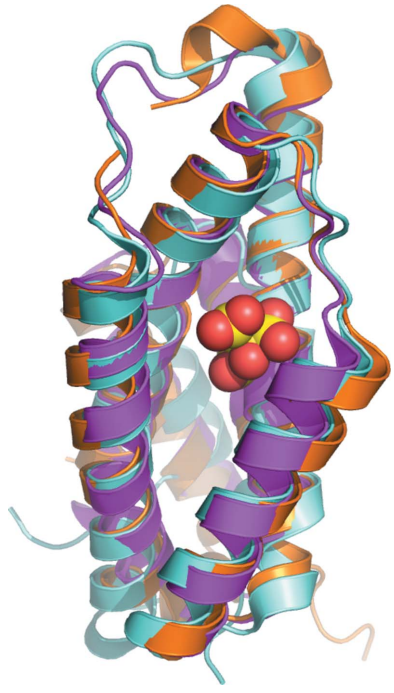

Figure 2
Superposed protomers of chorismate mutases with AroQγ topology from *B. thailandensis* (magenta; current study), *M. tuberculosis* (gold; PDB entry 2fp2; Okvist *et al.*, 2006) and *Y. pestis* (cyan; PDB entry 2gbb; Kim *et al.*, 2008). A citrate molecule (yellow and red spheres) sits in the substrate-binding cavity of the *Y. pestis* crystal structure.

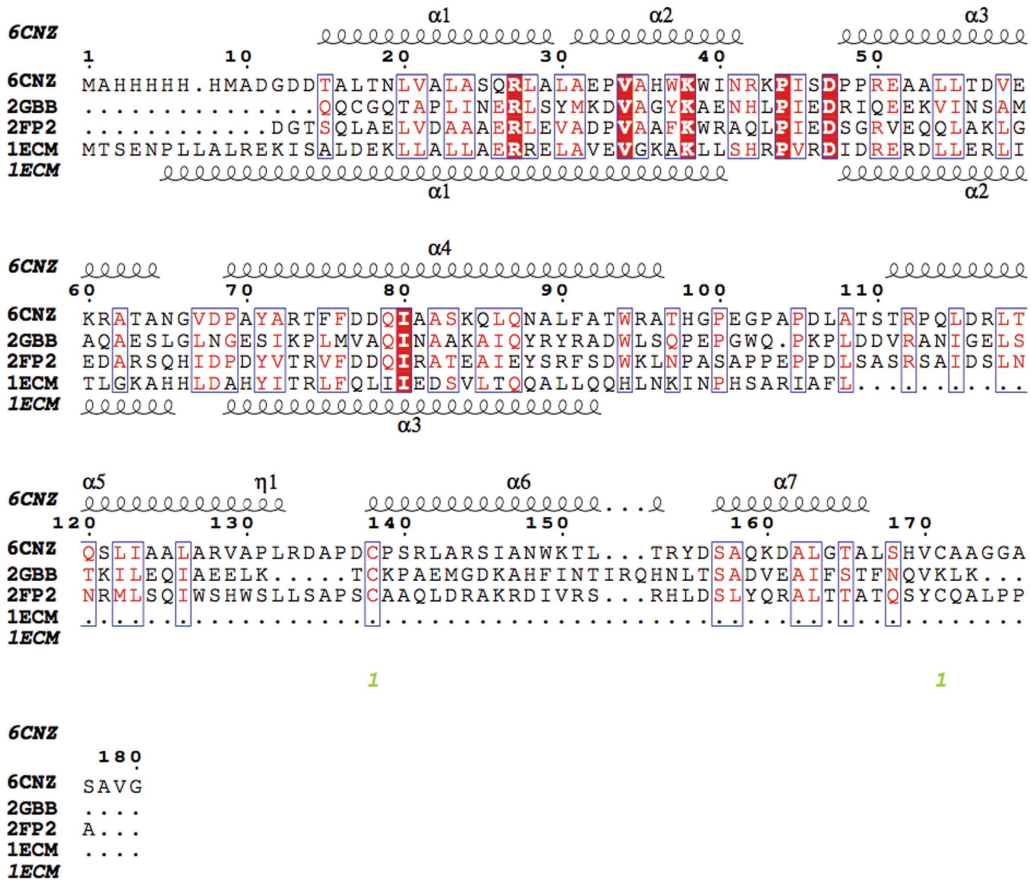

Figure 3
Structural and primary-sequence alignment of chorismate mutases from *B. thailandensis* (PDB entry 6cnz), *M. tuberculosis* (PDB entry 2fp2; Okvist *et al.*, 2006), *Y. pestis* (cyan; PDB entry 2gbb; Kim *et al.*, 2008) and *E. coli* (PDB entry 1ecm; Lee *et al.*, 1995). The secondary-structure elements shown are α-helices (α), 3_{10}-helices (η), β-strands (β) and β-turns (TT). Identical residues are shown in white on a red background and conserved residues are shown in red. This figure was generated using *ESPript* (Gouet *et al.*, 1999, 2003).

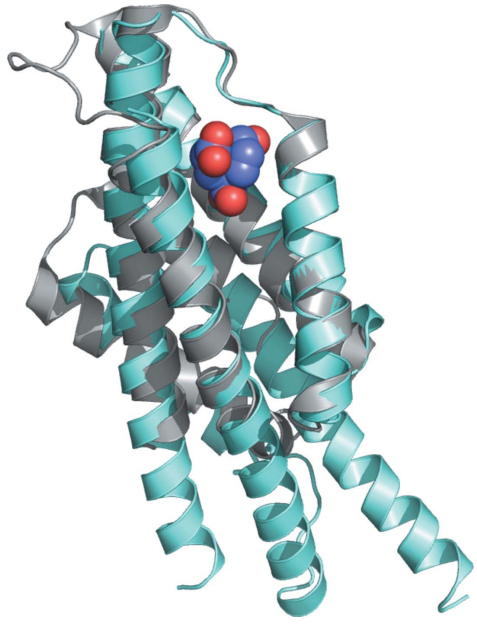

Figure 4
Superposition of chorismate mutase from *E. coli* (cyan; PDB entry 1ecm; Lee *et al.*, 1995) with that from *B. thailandensis* (gray); the transition-state analogue (blue and red spheres) in the active site is shown.

PDBeFold (http://www.ebi.ac.uk/msd-srv/ssm) analysis using the default threshold cutoffs of 70% for the percentage of the secondary structure of the target chain identified in the query protein and of the secondary structure of the query chain (Krissinel & Henrick, 2004). Of the 133 990 entries in the PDB, only three unique matches were identified at the default cutoff: chorismate mutases from *M. tuberculosis* (Okvist *et al.*, 2006; Kim *et al.*, 2006, Qamra *et al.*, 2006), *Yersinia pestis* (Kim *et al.*, 2008) and *B. phymatum* (PDB entry 5ts9; Asojo *et al.*, 2018).

The overall structure of each protomer of chorismate mutase from *B. thailandensis* follows the AroQγ topology as observed in the secreted chorismate mutases from *M. tuberculosis* (PDB entry 2fp2, 32% sequence identity; PDB entry 2f6l, 31% sequence identity; PDB entry 2ao2, 32% sequence identity; Okvist *et al.*, 2006; Kim *et al.*, 2006; Qamra *et al.*, 2006), *Y. pestis* (PDB entry 2gbb, 20% sequence identity; Kim *et al.*, 2008) and *B. phymatum* (PDB entry 5ts9, 33% sequence identity). The AroQγ topology is composed entirely of helices connected by short loops (Fig. 2). Despite having only 30% sequence identity, the members of the AroQγ subclass have a similar overall topology and conserved core helices (Fig. 2). The r.m.s.d.s on superposing C^{α} atoms of the *B. thailandensis*

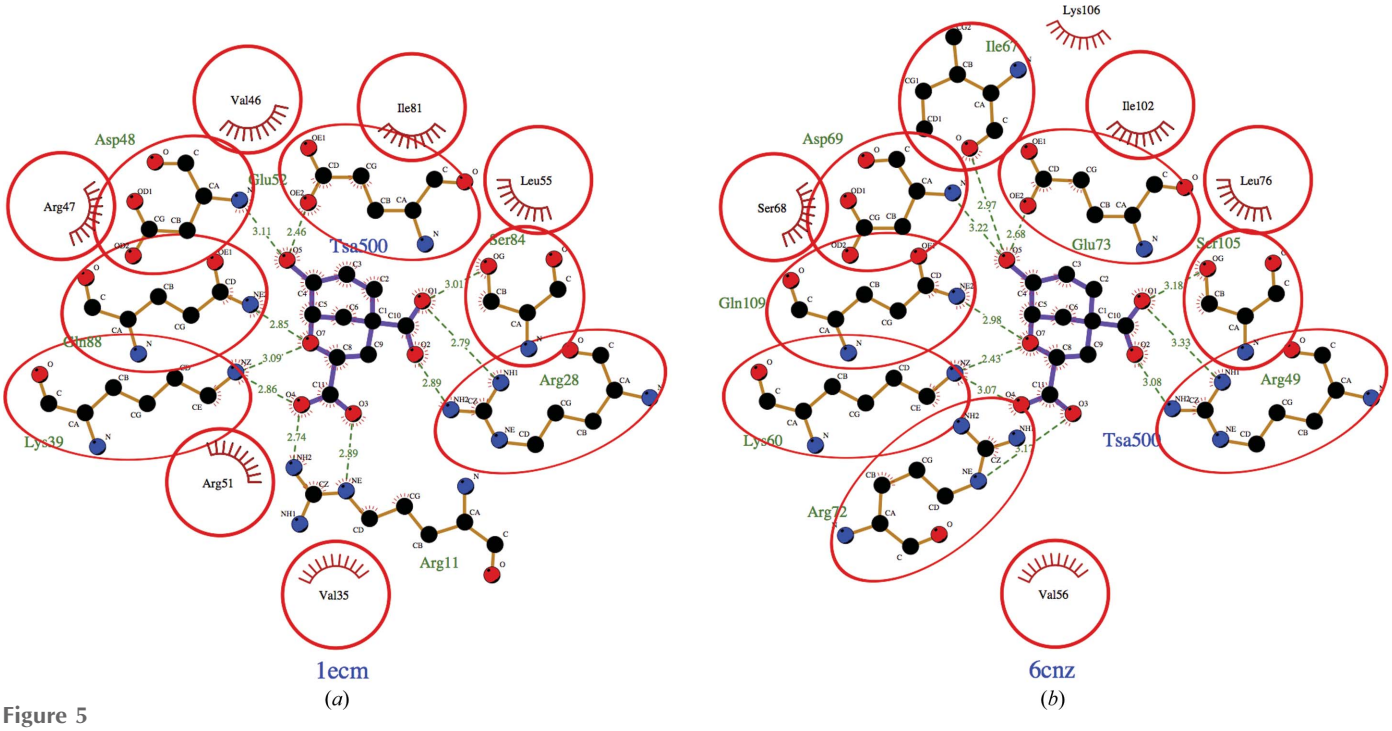

Figure 5
LigPlot diagrams reveal conserved residues in the substrate-binding sites of chorismate mutase from *E. coli* bound to a transition-state analogue (PDB entry 1ecm; Lee *et al.*, 1995) and of *B. thailandensis* chorismate mutase (PDB entry 6cnz) generated *via* an overlay with the *E. coli* structure.

protomer with the homologues from *B. phymatum*, *M. tuberculosis* and *Y. pestis* are 1.17 Å (over 158 amino acids), 1.18 Å (over 154 amino acids) and 1.36 Å (over 154 amino acids), respectively. As shown in the primary-sequence alignment (Fig. 3) and the structural overlay (Fig. 4), the *E. coli* chorismate mutase (Lee *et al.*, 1995) with AroQα topology has longer helices. These extended helices are in regions of low sequence homology between the different chorismate mutase subfamilies and are distant from the substrate-binding site.

While no reported structures of AroQγ chorismate mutases have substrates or substrate analogues in the active site, the crystal structure of the AroQα chorismate mutase from *E. coli* (PDB entry 1ecm; Lee *et al.*, 1995) was determined with a transition-state analogue (TSA). The *E. coli* protein does not have any appreciable sequence similarity to the *B. thailandensis* protein, but the amino-acid residues that make up the active site and are involved in substrate binding are conserved (Figs. 4 and 5). A *LigPlot* (Laskowski & Swindells, 2011; Wallace *et al.*, 1995) analysis of the interactions of the active site of *E. coli* chorismate mutase bound to a TSA and a model of *B. thailandensis* chorismate mutase generated *via* an overlay reveals a well conserved binding cavity. For example, based on this overlay with *E. coli* chorismate mutase bound to a TSA, we can predict that conserved residues Arg49, Lys60, Asp69, Gln73, Ser105 and Gln109 should bind to the TSA. Arg134 of the *B. thailandensis* chorismate mutase structure occupies a similar space to Arg11 of the *E. coli* enzyme, despite occurring in a different position in the primary sequence. The conservation of the active site of the enzyme suggests that broad-spectrum active-site inhibitors can be designed to target both AroQγ and AroQα chorismate mutases. We observed nitrate molecules bound in our crystal structure; for example, in all six protomers present in the asymmetric unit we observed a nitrate bound to Ser47, Trp171 and Gln181 and a second nitrate bound to Arg134. While the first site is not conserved and is therefore unlikely to be relevant for broad-spectrum drug development, the second site at Arg134 is significant since the equivalent residue in *M. tuberculosis* interacts with one of the carboxylates of the TSA. Thus, a nitrate isostere could be incorporated into the scaffold of a compound intended to mimic this interaction.

4. Conclusions

Despite sharing less than 33% sequence identity with homologous proteins, the structure of chorismate mutase from *B. thailandensis* reveals that it has a conserved AroQγ topology and substrate-binding cavity and could be targeted by inhibitors developed for these homologs.

Acknowledgements

We thank the SSGCID cloning and protein-production groups at the Center for Infectious Disease Research and at the University of Washington.

Funding information

The following funding is acknowledged: National Institutes of Health/National Institute of Allergy and Infectious Diseases (contract Nos. HHSN272200700057, HHSN272201200025C and HHSN272201700059C to Peter J. Myler). This research used resources of the Advanced Photon Source, a US

Department of Energy (DOE) Office of Science User Facility operated for the DOE Office of Science by Argonne National Laboratory under Contract No. DE-AC02-06CH11357. Use of the LS-CAT Sector 21 was supported by the Michigan Economic Development Corporation and the Michigan Technology Tri-Corridor (Grant 085P1000817).

References

Abell, C. (1999). *Comprehensive Natural Products Chemistry*, edited by O. Meth-Cohn, D. Barton & K. Nakanishi, Vol. 1, pp. 573–607. Amsterdam: Elsevier.

Agodi, A., Barchitta, M., Gianninò, V., Collura, A., Pensabene, T., Garlaschi, M. L., Pasquarella, C., Luzzaro, F., Sinatra, F., Mahenthiralingam, E. & Stefani, S. (2002). *J. Hosp. Infect.* **50**, 188–195.

Aslanidis, C. & de Jong, P. J. (1990). *Nucleic Acids Res.* **18**, 6069–6074.

Asojo, O. A., Subramanian, S., Abendroth, J., Exley, I., Lorimer, D. D., Edwards, T. E. & Myler, P. J. (2018). *Acta Cryst.* F**74**, 187–192.

Bryan, C. M., Bhandari, J., Napuli, A. J., Leibly, D. J., Choi, R., Kelley, A., Van Voorhis, W. C., Edwards, T. E. & Stewart, L. J. (2011). *Acta Cryst.* F**67**, 1010–1014.

Chen, V. B., Arendall, W. B., Headd, J. J., Keedy, D. A., Immormino, R. M., Kapral, G. J., Murray, L. W., Richardson, J. S. & Richardson, D. C. (2010). *Acta Cryst.* D**66**, 12–21.

Choi, R., Kelley, A., Leibly, D., Nakazawa Hewitt, S., Napuli, A. & Van Voorhis, W. (2011). *Acta Cryst.* F**67**, 998–1005.

Coggins, J. R., Abell, C., Evans, L. B., Frederickson, M., Robinson, D. A., Roszak, A. W. & Lapthorn, A. P. (2003). *Biochem. Soc. Trans.* **31**, 548–552.

Cui, Z., Zhu, B., Xie, G., Li, B. & Huang, S. (2016). *Rice Sci.* **23**, 111–118.

Emsley, P. & Cowtan, K. (2004). *Acta Cryst.* D**60**, 2126–2132.

Emsley, P., Lohkamp, B., Scott, W. G. & Cowtan, K. (2010). *Acta Cryst.* D**66**, 486–501.

Gouet, P., Courcelle, E., Stuart, D. I. & Métoz, F. (1999). *Bioinformatics*, **15**, 305–308.

Gouet, P., Robert, X. & Courcelle, E. (2003). *Nucleic Acids Res.* **31**, 3320–3323.

Haraga, A., West, T. E., Brittnacher, M. J., Skerrett, S. J. & Miller, S. I. (2008). *Infect. Immun.* **76**, 5402–5411.

Haslam, E. (1993). *Shikimic Acid: Metabolism and Metabolites.* Chichester: John Wiley & Sons.

Kabsch, W. (2010). *Acta Cryst.* D**66**, 125–132.

Kim, H. S., Schell, M. A., Yu, Y., Ulrich, R. L., Sarria, S. H., Nierman, W. C. & DeShazer, D. (2005). *BMC Genomics*, **6**, 174.

Kim, S.-K., Reddy, S. K., Nelson, B. C., Robinson, H., Reddy, P. T. & Ladner, J. E. (2008). *FEBS J.* **275**, 4824–4835.

Kim, S.-K., Reddy, S. K., Nelson, B. C., Vasquez, G. B., Davis, A., Howard, A. J., Patterson, S., Gilliland, G. L., Ladner, J. E. & Reddy, P. T. (2006). *J. Bacteriol.* **188**, 8638–8648.

Krissinel, E. & Henrick, K. (2004). *Acta Cryst.* D**60**, 2256–2268.

Laskowski, R. A. & Swindells, M. B. (2011). *J. Chem. Inf. Model.* **51**, 2778–2786.

Lebedev, A. A., Vagin, A. A. & Murshudov, G. N. (2008). *Acta Cryst.* D**64**, 33–39.

Lee, A. Y., Karplus, P. A., Ganem, B. & Clardy, J. (1995). *J. Am. Chem. Soc.* **117**, 3627–3628.

Limmathurotsakul, D. & Peacock, S. J. (2011). *Br. Med. Bull.* **99**, 125–139.

Mahenthiralingam, E., Baldwin, A. & Vandamme, P. (2002). *J. Med. Microbiol.* **51**, 533–538.

Mousdale, D. M. & Coggins, J. R. (1991). *Target Sites for Herbicide Action*, edited by R. C. Kirkwood, pp. 29–56. New York: Plenum.

Munack, S., Roderer, K., Ökvist, M., Kamarauskaite, J., Sasso, S., van Eerde, A., Kast, P. & Krengel, U. (2016). *J. Mol. Biol.* **428**, 1237–1255.

Murshudov, G. N., Skubák, P., Lebedev, A. A., Pannu, N. S., Steiner, R. A., Nicholls, R. A., Winn, M. D., Long, F. & Vagin, A. A. (2011). *Acta Cryst.* D**67**, 355–367.

Myler, P. J., Stacy, R., Stewart, L., Staker, B. L., Van Voorhis, W. C., Varani, G. & Buchko, G. W. (2009). *Infect. Disord. Drug Targets*, **9**, 493–506.

Nazmi, A. R., Lang, E. J. M., Bai, Y., Allison, T. M., Othman, M. H., Panjikar, S., Arcus, V. L. & Parker, E. J. (2016). *J. Biol. Chem.* **291**, 21836–21847.

Okvist, M., Dey, R., Sasso, S., Grahn, E., Kast, P. & Krengel, U. (2006). *J. Mol. Biol.* **357**, 1483–1499.

Qamra, R., Prakash, P., Aruna, B., Hasnain, S. E. & Mande, S. C. (2006). *Biochemistry*, **45**, 6997–7005.

Roberts, F., Roberts, C. W., Johnson, J. J., Kyle, D. E., Krell, T., Coggins, J. R., Coombs, G. H., Milhous, W. K., Tzipori, S., Ferguson, D. J., Chakrabarti, D. & McLeod, R. (1998). *Nature (London)*, **393**, 801–805.

Sawana, A., Adeolu, M. & Gupta, R. S. (2014). *Front. Genet.* **5**, 429.

Serbzhinskiy, D. A., Clifton, M. C., Sankaran, B., Staker, B. L., Edwards, T. E. & Myler, P. J. (2015). *Acta Cryst.* F**71**, 594–599.

Speert, D. P., Henry, D., Vandamme, P., Corey, M. & Mahenthiralingam, E. (2002). *Emerg. Infect. Dis.* **8**, 181–187.

Stacy, R., Begley, D. W., Phan, I., Staker, B. L., Van Voorhis, W. C., Varani, G., Buchko, G. W., Stewart, L. J. & Myler, P. J. (2011). *Acta Cryst.* F**67**, 979–984.

Studier, F. W. (2005). *Protein Expr. Purif.* **41**, 207–234.

Terwilliger, T. C., Grosse-Kunstleve, R. W., Afonine, P. V., Moriarty, N. W., Zwart, P. H., Hung, L.-W., Read, R. J. & Adams, P. D. (2008). *Acta Cryst.* D**64**, 61–69.

Vagin, A. & Teplyakov, A. (2010). *Acta Cryst.* D**66**, 22–25.

Wallace, A. C., Laskowski, R. A. & Thornton, J. M. (1995). *Protein Eng.* **8**, 127–134.

Whitlock, G. C., Estes, D. M. & Torres, A. G. (2007). *FEMS Microbiol. Lett.* **277**, 115–122.

Yabuuchi, E., Kosako, Y., Oyaizu, H., Yano, I., Hotta, H., Hashimoto, Y., Ezaki, T. & Arakawa, M. (1992). *Microbiol. Immunol.* **36**, 1251–1275.